Fast view-specific generation of high-definition holograms with enhanced quality

Antoine Lagrange, Antonin Gilles, Kevin Heggarty, Bruno Fracasso

Research Article | Vol. 32, No. 16 / 29 Jul 2024 / Optics Express 28821
Optics EXPRESS

Fast view-specific generation of high-definition holograms with enhanced quality

ANTOINE LAGRANGE,[1,2,*] ANTONIN GILLES,[1] KEVIN HEGGARTY,[2] AND BRUNO FRACASSO[2]

[1] Image Vision & Immersion Lab, Research and Technology Institute, 35510 Cesson-Sévigné, France
[2] Optics Department, IMT-Atlantique, Technopole Brest-Iroise, CS 83818, 29285 Brest, France
[*] antoine.lagrange@b-com.com

Abstract: Holography is often considered as the most promising immersive technology because it provides all the depth cues of the human visual system. Some limitations still need to be overcome such as the huge computational load of high-definition holograms and the noise introduced in the reconstructed scene during the quantization process. In this paper, we propose what we believe is a novel view-specific layer-based stereogram approach combined with a view-dependent error diffusion algorithm that aims to solve those limitations. This method selects the light waves of the 3D scene that reach a specific viewing area and leverages this particular configuration to apply an error diffusion algorithm. Two additional quality enhancement features are observed: the reduction of the conjugate order perceptibility and the increased brightness of the reconstructed scene. Numerical and optical experiments demonstrate the time savings and quality enhancements of our approach.

1. Introduction

Due to the recent progress in capture and visualization of 3D information, increasing interest is being shown in immersive technologies [1]. Most of the developed systems use stereoscopy to provide the depth information to observers, which consists in delivering different images to each eye [2]. However, this technique does not provide all the depth cues used by the human visual system (HVS), especially the accommodation cue. In a stereoscopic system, viewers focus their eyes on a plane at a fixed depth that does not correspond to the real depth of the represented objects. This mismatch, called the vergence-accommodation conflict, strongly decreases the 3D perception of the scene and leads to eye-strain and headaches [3].

Other technologies have been studied to overcome this issue. Among them, holography is often considered as the most promising. Indeed, it can provide all the depth cues of the HVS without any eye-strain [4]. To create the depth illusion, a hologram diffracts a light beam in such a way that the wave it scatters corresponds to the light emitted by a given 3D scene. Thus, viewers observing a hologram see the represented scene as if it were in front of them.

However, there are still some technological limitations concerning the numerical synthesis of 3D holograms. One of the main limitation is the huge amount of data that has to be processed to generate a hologram representing a scene of natural size. As holograms are based on diffraction, their pixels must have a size with the same order of magnitude as the wavelength of light. Thus, a large computer-generated hologram (CGH) with a wide viewing angle contains billions of pixels which implies that its generation process has a high time complexity. To speed-up calculations, methods based on look-up tables [5–7] and wavefront recording planes [8] have been introduced in the point-based paradigm. In polygon-based methods, the traditional algorithm [9] is improved by analytical approaches [10–12] that bring time savings. Layer-based methods have a lower time complexity than previous techniques because only a few layers are needed to describe

#531348 https://doi.org/10.1364/OE.531348
Journal © 2024 Received 28 May 2024; revised 2 Jul 2024; accepted 8 Jul 2024; published 25 Jul 2024

Optics EXPRESS

the 3D scene while preserving accurate depth cues [13,14]. Some techniques such as [15,16] improve further the computation time. However, layer-based methods encounter issues when computing high definition holograms having over 100 million pixels because the signal does not fit entirely in the memory. Moreover, view-dependent properties such as shading and occlusions are not included in these techniques and must be explicitly handled as in [17–20]. Holographic stereogram methods spatially partition a CGH into rectangular segments called hogels that angularly multiplex 2D views of the scene [21]. These techniques are computationally very efficient and handle view-dependent effects. However, this type of approach does not include the accommodation cue and smooth motion parallax. To improve the depth perception of holographic stereograms, phase-added methods [22,23], ray-sampling plane [24,25] and diffraction specific coherent panoramagram [26] have been introduced to better approximate the wavefront in the hologram plane. Furthermore, the holographic stereogram method and layer-based approach have been merged [27] to compute CGHs with accurate depth cues and low time complexity. Even if this algorithm is fast and provides an accurate reconstruction, further improvements are needed to generate high definition holograms in real-time.

Another limitation lies in the fact that while state-of-the-art methods often generate complex-valued holograms with floating-point amplitude and phase values, CGHs must be converted to pure phase or amplitude signals with quantized levels to be displayed. Indeed, current holographic displays only modulate the amplitude or the phase of the incident light and have a limited number of bits per pixel [28]. During this process, part of the signal information is lost which introduces distortion in the reconstructed scene. To enhance the visualisation quality, Iterative Fourier transform algorithms (IFTAs) offer great results [29]. However, these methods are remarkably costly in time due to their iterative nature that relies on 2D Fourier transforms. Double phase approaches are another solution [30,31]. Nevertheless, in these methods, each phase value of the object wave is encoded using two hologram pixels, dividing by two the hologram size. A fast and simple technique is the well-known error diffusion algorithm which rejects the quantization noise outside of the reconstructed area by propagating the quantization error of a pixel to its neighbours according to diffusion weights [32–34]. In conventional generation approaches, the quantization noise is usually distributed in the high spatial frequencies of the hologram. As these frequencies are limited by the pixel pitch of the hologram, the quantization noise is visible on the border of the reconstruction plane. Thus, in these methods, the quality enhancement effect of the error diffusion algorithm is limited.

To speed-up the computation time, SeeReal presented a view-specific synthesis approach [35] which generates a hologram only for a specific viewing area. However, their method relies on a point-based algorithm which has a high time complexity and, to the best of our knowledge, the visual quality enhancement of these holograms has never been studied. In this paper, we propose a novel view-specific layered holographic stereogram approach combined with a view-dependent error diffusion algorithm to calculate CGHs. Our approach overcomes both the time complexity limitation associated with the generation of high definition holograms and the quality enhancement limitation of the error diffusion algorithm applied to conventional generation techniques. Indeed, as a view-specific hologram is only a subset of a multi-view hologram in phase space [36], the amount of information to be processed is drastically reduced which decreases the computation time. Moreover, in our method, the reconstruction plane of each hogel contains the information of the 3D scene in a restricted area. In this way, the quantization noise is placed in the free areas with a view-dependent error diffusion algorithm based on [32] which implies that high spatial frequencies are not added to the hologram. Our approach also brings two additional quality enhancements: the imperceptibility of the conjugate order and the increased brightness of the reconstructed scene. Furthermore, since our paper is about high definition holograms that have over 100 million pixels, they are engraved with the photoplotter presented in [37]. Indeed, current liquid crystal displays (LCDs) and digital micro-mirror devices

Optics EXPRESS

(DMDs) have a limited number of pixels. Otherwise, our method is intended to be combined with an eye tracking system to give observers the same freedom as if they were visualizing a multi-view hologram.

The following of this paper is organized as follows: Section 2 gives an overview of our method, Section 3 presents the view-specific hologram generation approach and Section 4 provides details on the view-dependent error diffusion method used to convert and quantize the resulting hologram. Finally, experimental results are analyzed in Section 5.

2. Overview

Our method speeds up and enhances the reconstruction quality of the layered holographic stereogram technique [27] by selecting a specific viewing area. The block diagram of Fig. 1 explains the generation process of our method, whose steps are detailed in Sections 3 and 4. The hologram is first spatially decomposed into several blocks called hogels. Their definition determines the trade-off between spatial and angular resolutions as in standard stereogram approaches. Afterwards, for each hogel, an intensity map and a depth map are obtained by perspective rendering of the scene from a virtual camera positioned at the center of the block. To select the light waves the observer perceives, the depth and intensity maps are cropped according to the viewer and the hogel position. Then, for each block, the 3D scene is reconstructed from the acquired 2D-plus-depth image as a set of parallel depth layers and the light waves they scatter are propagated with Fresnel diffraction and superimposed in the hogel plane. To display the hologram, the computed hogels are converted to phase-only signals and quantized. To this end, we use a view-dependent error diffusion algorithm based on [32] to diffuse the quantization noise outside of the visualisation window. By considering Fig. 1, a multi-view approach is obtained by deleting the "Viewing area selection" and "Conversion and quantization" steps. In this case, the propagation of light waves from the scene to the hogels is more costly and the hologram quality decreases. For the sake of clarity, all the equations in this paper are expressed in 1D as the generalisation to 2D is straightforward. The coordinate system is presented in Fig. 2, where the eye represents an observer viewpoint.

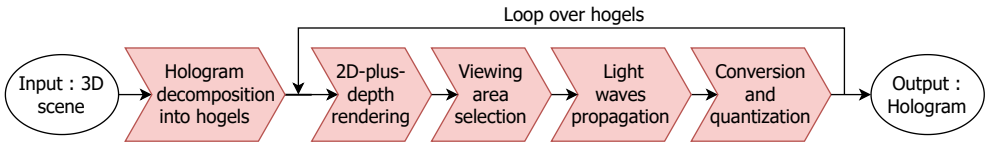

Fig. 1. Block diagram of the proposed method.

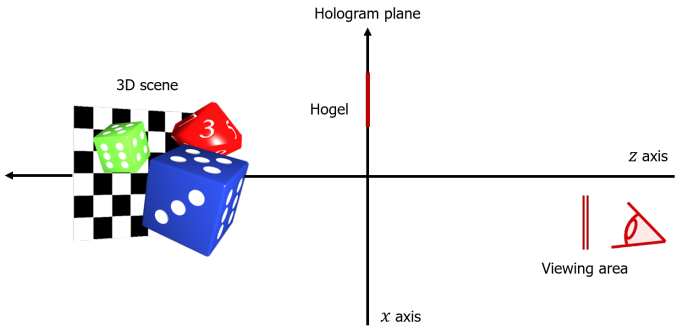

Fig. 2. Diagram of the coordinate system.

Optics EXPRESS

3. View-specific hologram generation

3.1. 2D-plus-depth rendering

For each hogel, a depth map and an intensity map are rendered from the 3D scene using a virtual camera whose projection center is placed at the center of the block with a field-of-view of

$$\theta = 2\arctan\left(\frac{\lambda}{2\delta x}\right), \tag{1}$$

where λ is the wavelength of the light source and δx is the sampling size of the hologram. The optical axis of the virtual camera is perpendicular to the hologram plane. Since the position of the camera varies from one hogel to the others, view-dependent effects such as occlusions and specular reflections are synthesized in the rendered 2D-plus-depth images without additional processing. Moreover, the observer is located away from the hologram plane and therefore perceives the light waves scattered by several hogels at the same time. In this way, this viewer sees a blending of light waves propagating from these blocks, which allows a smooth continuity between views. Furthermore, the position and orientation of the virtual camera do not vary according to the observer's viewpoint. Indeed, the selection of the light waves reaching the visualisation window is decorrelated from the acquisition of the 2D-plus-depth images.

3.2. Viewing area selection and light waves propagation

The diagram of Fig. 3 represents an observer looking towards the hologram plane and defines the diffraction angles of the perceived light waves which lie between

$$\theta_{\min} = \arctan\left(\frac{\Delta_{\min}}{d}\right) \quad \text{and} \quad \theta_{\max} = \arctan\left(\frac{\Delta_{\max}}{d}\right), \tag{2}$$

where $\Delta_{\min}$ and $\Delta_{\max}$ are the maximum and minimum distances between a hogel and the viewing area and d is the distance between the observer and the hologram. This interval can be converted to hologram spatial frequencies with the first-order grating equation,

$$\sin(\theta_d) = \sin(\theta_i) + f\lambda, \tag{3}$$

where θ_i and θ_d are respectively the angles of incidence and diffraction and f is the corresponding spatial frequency. Thus, for each hogel, only the light waves whose spatial frequency lie between

$$f_{\min} = \frac{\sin(\theta_{\min}) - \sin(\theta_i)}{\lambda} \quad \text{and} \quad f_{\max} = \frac{\sin(\theta_{\max}) - \sin(\theta_i)}{\lambda} \tag{4}$$

have to be considered to generate a hologram for a specific viewing area. In the discrete domain, these spatial frequencies have the following pixel coordinates

$$\zeta_{\min} = \left(f_{\min}\delta x + \frac{1}{2}\right)N \quad \text{and} \quad \zeta_{\max} = \left(f_{\max}\delta x + \frac{1}{2}\right)N, \tag{5}$$

where N is the hogel definition.

To generate a hogel, the associated intensity map is sliced into several layers according to the corresponding depth map. The light waves scattered by each layer $U_l(p)$ are propagated towards the hogel plane with the discrete Fresnel diffraction formula,

$$U_h(n) = \frac{e^{jkz}}{j\lambda z} e^{j\frac{k}{2z}n^2\delta x^2} \sum_{p=0}^{N-1} U_l(p) e^{j\frac{k}{2z}p^2\delta\xi^2} e^{j2\pi\frac{np}{N}}, \tag{6}$$

where $k = \frac{2\pi}{\lambda}$ is the wavenumber of the light source, z is the depth of a layer, δx and $\delta\xi$ correspond respectively to the sampling size in the destination and source planes. The field $U_h(n)$ can be

Optics EXPRESS

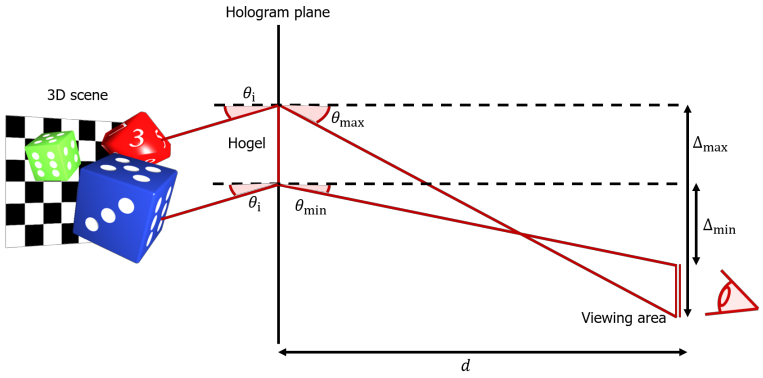

Fig. 3. Maximum and minimum diffraction angles of light waves received by an observer.

understood as a sum of plane waves whose discrete spatial frequency coordinates are given by p. The Fresnel propagation formula links the object and hologram planes by an inverse Fourier transform, which means that p is the spatial coordinate of the object plane and the spatial frequency coordinate of the hologram plane. As only the plane waves with discrete spatial frequency coordinates lying between $\zeta_{\min}$ and $\zeta_{\max}$ are needed to generate the hogel, Eq. (6) can be rewritten as follows

$$U_h(n) = \frac{e^{jkz}}{j\lambda z} e^{\frac{k}{2z}n^2\delta x^2} \sum_{p=\zeta_{\min}}^{\zeta_{\max}} U_l(p) e^{j\frac{k}{2z}p^2\delta\xi^2} e^{j2\pi\frac{np}{N}}. \tag{7}$$

Thus, the amplitude of the light waves is $U_l(p)$ which means that bounding the sum in Eq. (7) is equivalent to cropping the intensity map from $\zeta_{\min}$ to $\zeta_{\max}$ as shown in Fig. 4. The reduction of the intensity map size decreases the number of layers from which light waves scatter to the hogel plane. In this way, the number of operations to compute a hogel is drastically reduced, which speeds up the overall computation effort.

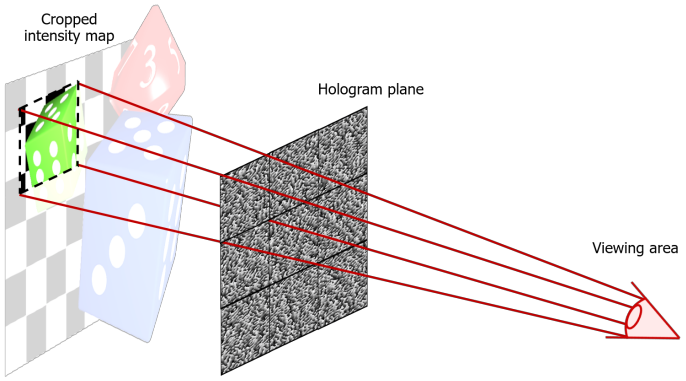

Fig. 4. Selection of the light waves perceived from a specific viewing area.

Moreover, the selection of a restricted set of light waves improves the quality of the reconstruction by decreasing the perceptibility of the conjugate order and by increasing the brightness of the reconstruction. The conjugate order of the reconstructed scene always appears when a hologram is displayed on an optical system due to the quantization of the hologram values. This artefact

Optics EXPRESS

decreases the viewing comfort of an observer as it is superimposed on the reconstructed scene in an on-axis configuration. The conjugate light waves of the conjugate order are associated with light waves emitted by the 3D scene. In the view-specific generation process, light waves that are not reaching the viewing area are not included in the hologram. Therefore, the corresponding conjugate light waves do not scatter to the visualization window, which reduces the perceptibility of the conjugate order, as shown in Fig. 5. Furthermore, in a multi-view hologram, the light source is diffracted in every direction which divides its intensity between each view. Conversely, in the view-specific case, the set of views is limited, which implies that the light source is concentrated in these areas.

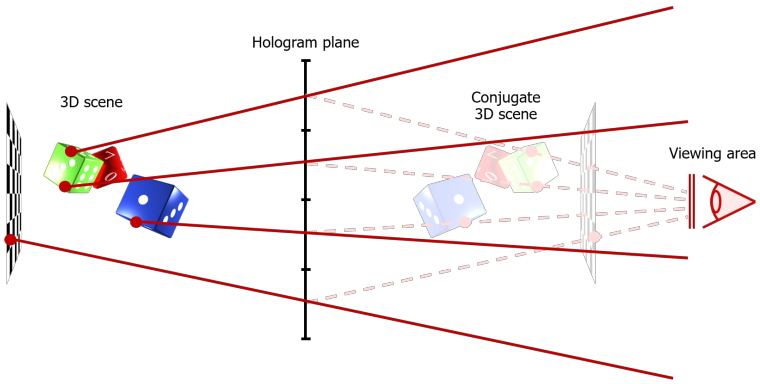

Fig. 5. Light red dotted lines represent conjugate light waves and dark red solid lines correspond to the 3D scene light waves. Dark red points belong to the 3D scene and light red points are virtual points of the conjugate order. This diagram illustrates the perceptibility reduction of the conjugate order for view-specific holograms.

4. Conversion and quantization

4.1. Signal window error diffusion

Once the complex-valued light wave has been computed in the hologram plane for every hogel, it should be converted to an amplitude-only or phase-only hologram with quantized values. During this process part of the information is lost which creates quantization noise in the reconstruction plane. The error diffusion algorithm is a well-known halftoning method to reduce this noise. It distributes the quantization error of a pixel to its neighbours according to diffusion weights in order to compensate for the errors created by the quantization process. It is a one step technique which allows a fast processing of the entire hologram [38,39]. In most methods [33,34], the error is propagated according to Floyd-Steinberg coefficients which reject the quantization noise from the center of the reconstruction plane. However, these approaches do not allow a precise placement of the quantization noise. Thus, to overcome this issue, the signal window error diffusion algorithm [32] proposes an alternative approach to compute the diffusion weights. In this method, these coefficients are equal to the Fourier transform of a mask function which indicates where the quantization noise must be placed. In multi-view hologram generation methods, all the reconstruction plane contains information. Moreover, the quantization noise cannot be put beyond this field due to the pixel size restriction. Hence, some quantization noise is still visible in the reconstruction.

Optics EXPRESS

4.2. View-dependent error diffusion

To reduce the high spatial frequencies in the hologram and enhance the quality of the reconstruction, we propose a new view-dependent error diffusion algorithm based on the signal window technique which leverages the view-specific generation configuration. In the view-specific paradigm, only part of a hogel's reconstruction plane is visible from the visualisation window. Therefore, the signal window error diffusion algorithm is applied on each hogel and the diffusion weights are computed to reject the quantization noise outside of regions of interest that contain information on the 3D scene and to limit the high spatial frequencies in the hogel. There are two regions of interest in the reconstruction plane: the target area, which is visible through the considered hogel by an observer in the visualisation window, defined by the frequency coordinates range

$$\zeta_{\min} < p < \zeta_{\max}, \tag{8}$$

and the conjugate area, which is symmetric to the target area according to the center of the reconstruction plane, defined as

$$N - \zeta_{\max} < p < N - \zeta_{\min}. \tag{9}$$

The quantization noise must not lie in the target area because this region is seen by the viewer, and should also stay outside of the conjugate area as the conjugate light waves which propagate from this area are visible from the viewing area. Otherwise, to restrict the high frequencies in the hogel the quantization noise must be rejected from the following region

$$p < \frac{N}{2}\left(1 - \frac{\delta x}{\delta \mathrm{fr}_{\min}}\right) \quad \text{and} \quad p > \frac{N}{2}\left(1 + \frac{\delta x}{\delta \mathrm{fr}_{\min}}\right). \tag{10}$$

where $\delta \mathrm{fr}_{\min}$ is the minimum size of fringes in the hogel. Indeed, areas close to the edges of the reconstruction plane correspond to large diffraction angles that must be filtered. Figure 6 illustrates these explanations by providing a visual understanding of the quantization noise location in the reconstruction plane. This VDED (view-dependent error diffusion) algorithm allows to place the quantization noise in a defined spatial frequency interval according to a position in the hologram which is equivalent to place this noise in specific views.

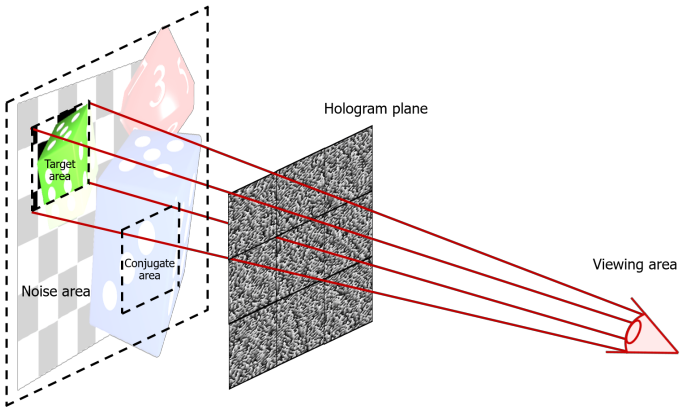

Fig. 6. The position of the quantization noise when the signal window error diffusion algorithm is applied on a hogel.

The diffusion weights associated to a hogel are equal to the Fourier transform of a mask which indicates where the quantization noise should be placed in the corresponding reconstruction

Optics EXPRESS

plane and are expressed as follows

$$\begin{aligned} w(n) &= \mathcal{F}\left\{m_{\text{ta}}(p) + m_{\text{ca}}(p) + m_{\text{hf}}(p)\right\}(n) \\ &= M_{\text{ta}}(n) + M_{\text{ca}}(n) + M_{\text{hf}}(n), \end{aligned} \tag{11}$$

where m_{ta} is the mask associated with the target area, m_{ca} is the mask which defines the conjugate area, m_{hf} is the mask which bounds the high frequencies in the hologram and $\mathcal{F}$ is the Fourier transform operator. The positions of the target and conjugate areas vary from hogel to hogel which implies that the diffusion weights must be computed for each block. Nevertheless, each set of weights should not be calculated with a fast Fourier transform (FFT) due to its noticeable time complexity. Indeed, the masks m_{ta} and m_{ca} can be computed by shifting a reference mask m_{ref} by a distance of p_{tr} and $-p_{\text{tr}}$ along the x axis, respectively. Thus, according to the shift theorem of the Fourier transform, the diffusion weights can be obtained such that

$$w(n) = M_{\text{ref}}(n)(e^{-j2\pi\frac{p_{\text{tr}}n}{N}} + e^{j2\pi\frac{p_{\text{tr}}n}{N}}) + M_{\text{hf}}(n) \tag{12}$$

where M_{ref} are the weights associated to the reference mask m_{ref}.

Once the diffusion weights of a hogel are computed, the quantization error of each pixel is calculated and then diffused to its neighbours. During this process, the hologram values can be accessed in different orders that are described in [40,41]. The quantization error of pixel n is defined as

$$e(n) = U_h(n) - q(n), \tag{13}$$

where $q(n)$ depends on the error of its neighbours, such that

$$q(n) = Q(U_h(n) + \sum_{k\in\Omega} w(k)e(n-k)). \tag{14}$$

The operator Q applies the quantization. The domain Ω is the domain of diffusion and corresponds to the pixels that have not been quantized yet. This algorithm is recursive and its complexity is $\Theta(Nk_w)$, where k_w is the number of weights.

To sum up, the first step of the view-dependent error diffusion algorithm is to compute the quantization noise masks. Then, the hologram is divided in several blocks. For each of them, a set of diffusion weights is computed according to the hogel position by applying the shift theorem of the Fourier transform on the masks. The last stage is to apply the signal window error diffusion (SWED) on each hogel with the computed weights. This process is illustrated in Fig. 7. Furthermore, while in the signal window technique, a set of diffusion weights is computed for the entire signal, in the view-dependent algorithm, each hogel has its own set of coefficients. Hence, in our approach, the quantization error is diffused differently according to the position of the pixels which means that the quantization noise is only visible for specific locations of the observer. By contrast, in the signal window technique, the quantization noise is located in the same area of the reconstruction for all viewpoints.

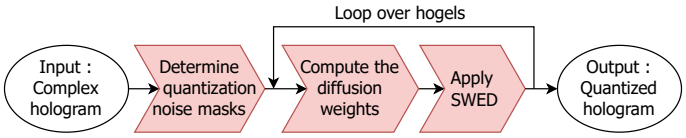

Fig. 7. Block diagram of the view-depend error diffusion algorithm.

Optics EXPRESS

5. Experimental results

5.1. Scene and hologram calculation parameters

The generation parameters of the phase-only holograms are described in Table 1. The field-of-view of 25°is limited by the minimum fringe size according to Eq. (1). To reduce artefacts when engraving the holograms with the photoplotter presented in [37], we set the minimum fringe size to 1.5µm. After several tests, a hogel size of 2048 × 2048 pixels appears as a good balance between angular and spatial resolutions. Furthermore, since high definition holograms having over 100 million pixels cannot be displayed on LCDs or DMDs, they are often engraved with lithography systems that are mostly binary [42]. However, reconstructions of binary holograms suffer from quantization noise and conjugate order. Hence, holograms in the experiment are binary to demonstrate the efficiency of our algorithm in the worst case scenario.

Table 1. Parameters of the generated holograms.

Parameter	Value
Pixel pitch	750nm
Fringe size	1.5µm
Field of view	25°
Hogel size	2048 × 2048 pixels
Wavelength	635nm
Modulation	Phase-only

The test scene is composed of 4 dices and a checkerboard as described in Table 2. The hologram is composed of 24k × 24k pixels and the viewing area is located on its right side. In Section 5.3, the number of pixels of the hologram varies and, in Section 5.5, its size is set to 30k × 20k pixels. Therefore, the scene objects are scaled proportionally. Moreover, light waves are propagated under paraxial approximation using the Fresnel diffraction formula. However, as the propagation is done per hogel, the distance between the 3D scene and the hologram is only restricted by the size of the hogels as detailed in Section 5.2.

Table 2. Parameters of the 3D scene.

Object	Size (mm)	Depth (cm)
Hologram	18.4 × 18.4	0
Viewing area	4.6 × 4.6	-3.6
Checkerboard	14.7 × 18.4	10.3
Top left dice	6 × 6 × 6	9.7
Bottom left dice	8 × 8 × 8	9.1
Top right dice	6 × 6 × 6	8.5
Bottom right dice	6 × 6 × 6	8.1

5.2. Validity of the Fresnel approximation

The paraxial approximation simplifies the scattering of light waves but is limited to small diffraction angles compared to the propagation distance. According to [43], a sufficient condition to obtain accurate results is the following

$$z^3 \gg \frac{\pi}{4\lambda}\left[(x-\xi)^2+(y-\eta)^2\right]^2_{\max}. \tag{15}$$

Optics EXPRESS

By making the assumption that the hologram and the object plane are squared and defining Δ_h and Δ_o as their width, respectively, Eq. (15) is rewritten as follows

$$z^3 \gg \frac{\pi}{4\lambda}\left[\left(\frac{\Delta_h+\Delta_o}{2}\right)^2+\left(\frac{\Delta_h+\Delta_o}{2}\right)^2\right]^2 \tag{16}$$

$$\gg \frac{\pi}{\lambda}\left(\frac{\Delta_h+\Delta_o}{2}\right)^4. \tag{17}$$

The size of the object plane Δ_o depends on the field of view which is computed as in Eq. (1). However, in the experiments, the field of view is restricted according to the fringe size Δ_{fr} which gives

$$\theta = 2\arctan\left(\frac{\lambda}{2\Delta_{fr}}\right). \tag{18}$$

The fringe size controls the field of view independently of the pixel pitch. This technique forces the diffraction patterns of the hologram to be smooth enough to ensure an accurate etching process. The width of the object plane is then given by

$$\Delta_o = 2z\tan(\frac{\theta}{2}) \tag{19}$$

$$= \frac{z\lambda}{\Delta_{fr}} \tag{20}$$

Therefore, according to Eq. (15), the minimal fringe size is equal to

$$\Delta_{fr}^{min} = z\lambda\left(2\sqrt[4]{\frac{z^3\lambda}{\pi}}-\Delta_h\right)^{-1} \tag{21}$$

$$\approx 9.1\mu m, \tag{22}$$

where λ and Δ_h are defined in Table 1 and z is the distance of the closest object in Table 2.

However, it is also stated in [43] that the condition in Eq. (15) is overly stringent. To quantify the errors that appear when this condition is not met, the fringe size is set to 1.5µm. Then, points are propagated with and without paraxial approximation and reconstructed with the angular spectrum method which is accurate. Several 1D tests were run in which each point is located at a specific distance from the optical axis. The errors are presented in Table 3. Graphs in Fig. 8 highlight the position errors of the reconstructed points propagated with the paraxial approximation. In Fig. 9, the reconstructed points scattered with Fresnel formula are shifted to study their focus errors. The position errors are computed by measuring the distance between the points propagated with the angular spectrum and the Fresnel formula. The focus errors are quantified by measuring the extra width of the paraxial points. Hence, the position errors are at most three order of magnitude smaller than the distance between the observer and the scene and are directed towards the edges of the object plane. Besides, the width of the paraxial points are at most two times larger than the non paraxial points. All errors decrease when points are getting closer to the optical axis. With our generation parameters, not respecting Eq. (15) only creates small stretches and a little blur on the edges of the reconstruction plane which are not significant as shown in the following sections.

Moreover, increasing the fringe size is equivalent to a high frequency cut-off which is very strong if Eq. (15) has to be satisfied. Such an operation greatly crops the scene as shown in Fig. 10, which decreases the quality of the reconstruction. Thus, we consider that in 3D visualization techniques, it is important to have a broad field of view even if it creates small reconstruction errors.

Optics EXPRESS

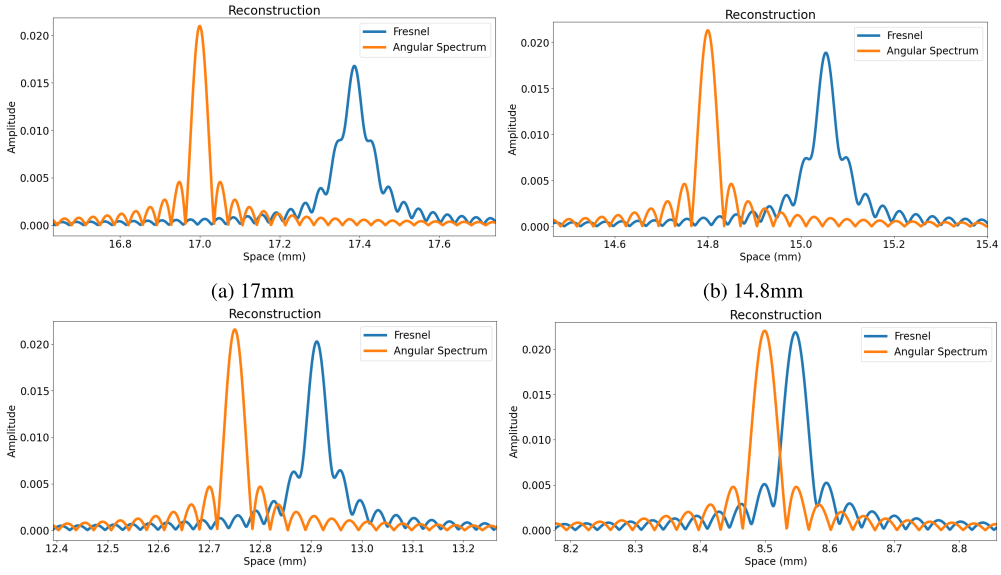

(a) 17mm (b) 14.8mm

(c) 12.75mm (d) 8.5mm

Fig. 8. Reconstruction of points scattered with the Fresnel approximation (blue line) and the angular spectrum (orange line) at different distances from the optical axis.

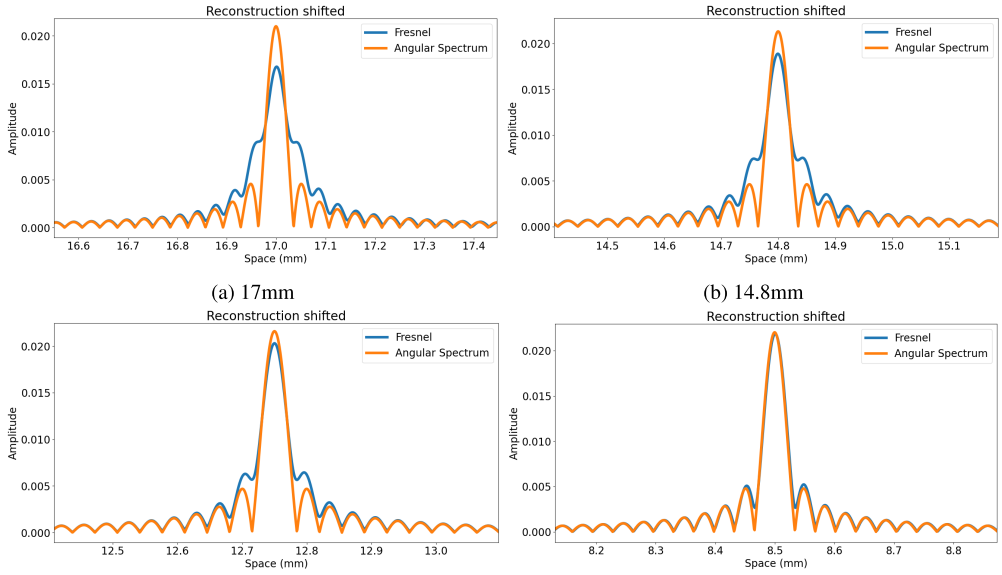

(a) 17mm (b) 14.8mm

(c) 12.75mm (d) 8.5mm

Fig. 9. Reconstruction of points scattered with the Fresnel approximation (blue line) and the angular spectrum (orange line) at different distances from the optical axis. Reconstructed points are shifted to evaluate their size.

Optics EXPRESS

Table 3. Errors induced by the paraxial approximation for points at different distances from the optical axis.

Position (mm)	Shift (mm)	Defocus (mm)
17	0.387	0.06
14.8	0.25	0.05
12.75	0.15	0.04
8.5	0.046	0

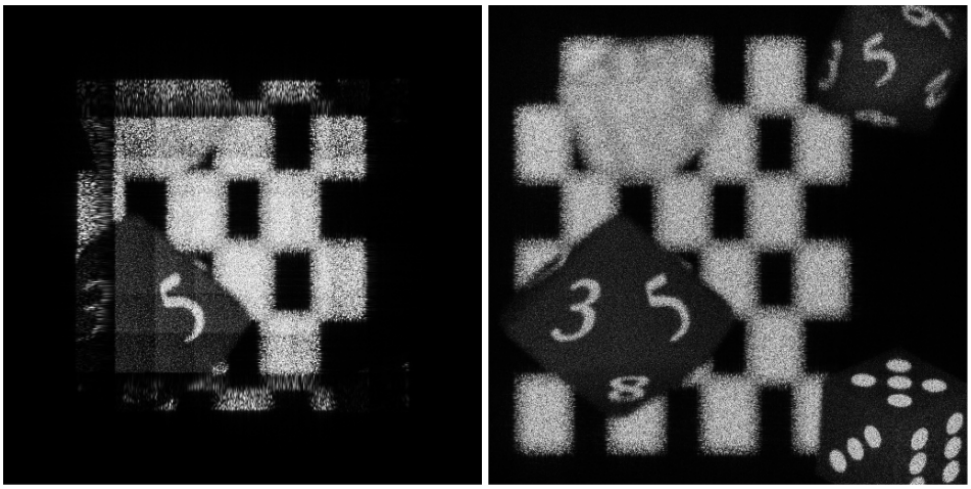

Fig. 10. Reconstruction of a 3D scene for different fringe sizes.

5.3. Numerical computation

Our method was implemented as a C++ Unity plugin on a PC system including an Intel Core i9-9900X operating at 3.5GHz, a 32GB random access memory (RAM) and a NVIDIA GeForce RTX 2080 Ti graphics card. To evaluate the speed up brought by our approach, we compared it with a graphics processing unit (GPU) implementation of the layered holographic stereogram approach [27] quantized with a truncation technique, called multi-view approach in the following. Moreover, the number and position of the layers are chosen according to the structure of the scene by means of k-means clustering, as proposed in [44].

To observe how the computation time varies according to the hologram size, the visualisation window is set to 4.6×4.6 mm to cover the size of a human pupil in bright light. Table 4 highlights that the number of layers per hogel is far less in the view-specific algorithm than in the multi-view one. Indeed, the depth and intensity maps are cropped in this approach which reduces the number of different depth values and therefore the number of depth planes for a hogel. Furthermore, for some hogels, no computation is required as their entire light field does not reach the visualisation window. In this way, the number of loading operations, addition and FFT decreases, which reduces drastically the computation time. Table 5 shows that the view-specific hologram generation process is much faster than the multi-view computation as it provides up to 94% speed up. This table also emphasizes that time savings increase as the hologram becomes wider. Indeed, the size of the viewing window does not depend on the hologram size. Hence, hogels located on the edges of the hologram are empty since the 3D scene is not visible through them from the visualisation window. Consequently, the average number of layers

Optics EXPRESS

per hogel decreases which means that the hologram computation is accelerated. However, the quantization is particularly slow because our algorithm is implemented on the central processing unit (CPU) and not optimized yet. In future work, we will study the parallelization of our proposed view-dependent error diffusion algorithm to implement it on a GPU. Indeed, state-of-the-art GPU implementations of the conventional error diffusion method are able to process a signal of 2048 × 2048 pixels in 1ms [45]. Therefore, we expect huge improvements in calculation time.

Table 4. Mean number of layers per hogel and percentage of null hogels according to the hologram definition for a viewing area of 4.6 × 4.6 mm.

Definition (pixels)	Multi-view [27]	Proposed approach	
	Layers	Layers	Null hogels (%)
16k × 16k	39.7	9.0	54.7
32k × 32k	39.7	3.5	77.3
65k × 65k	39.7	1.5	85.4
98k × 98k	39.7	1.0	88.2
131k × 131k	39.7	0.7	89.5

Table 5. Computation time according to the hologram definition for a viewing area of 4.6 × 4.6 mm.

Definition (pixels)	Multi-view [27] (s)	Proposed approach (s)	Quantization (s)
16k × 16k	2.43	0.60	15.5
32k × 32k	9.71	1.21	31.8
65k × 65k	38.85	2.87	82.9
98k × 98k	87.41	5.30	149.2
131k × 131k	156.73	8.50	221.2

The impact of the size of the viewing area on the computation time is studied by fixing the hologram definition to 24k × 24k pixels while the visualization window size varies. Table 6 emphasizes that the computation time decreases as the viewing area becomes tighter. Indeed, the depth map is cropped to a small size when the visualisation window is small, and therefore contains far less different values than the initial depth map. Thus, the mean number of layers per hogel decreases and the percentage of null hogels increases which saves a considerable amount of time.

Table 6. Mean number of layers per hogel, percentage of null hogels and computation time according to the viewing area size for a 24k × 24k pixels hologram.

Area size (mm)	Layers	Null hogels (%)	Generation (s)	Quantization (s)
9.2	11.3	52.1	1.65	37.3
6.9	8.3	57.6	1.27	33.4
4.6	4.9	72.9	0.86	20.9
2.3	2.9	79.2	0.6	16.3
1.2	1.9	83.3	0.45	13.2

Figure 11 shows three binary hogels, the first one has been extracted from a multi-view hologram and the others from view-specific holograms. The first two hogels were quantized with a truncation technique and the last hogel was quantized with the view-dependent error diffusion algorithm. Fringes in Fig. 11(a) have a uniform size and orientation because this hogel was generated with all the set of frequencies. In contrast, the fringes of the view-specific hogels get

Optics EXPRESS

closer to a grating since the selected light waves have frequencies lying in the same interval. In Fig. 11(c), the fringes are thinner than in Fig. 11(b) because the hogel was quantized with the view-dependent error diffusion algorithm. However, these fringes stay larger than those of Fig. 11(a).

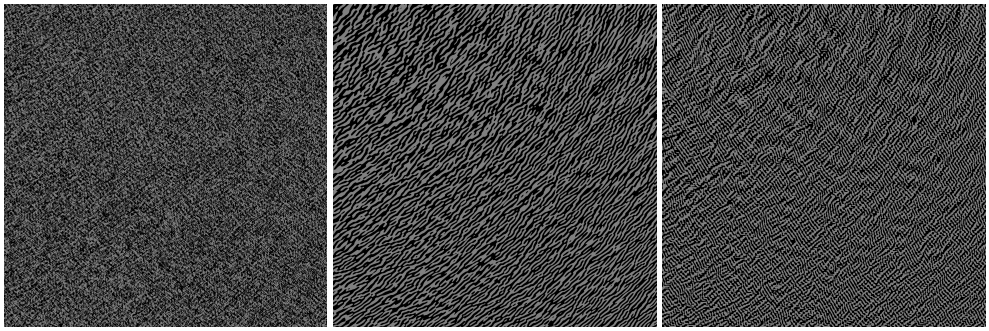

(a) Multi-view (b) View-specific (c) View-specific VDED

Fig. 11. (a) Hogel of a multi-view hologram quantized with a truncation method, (b) hogel of a view-specific hologram quantized with a truncation method and (c) hogel of a view-specific hologram quantized with the view-dependent error diffusion. Each hogel is a binary-phase signal.

5.4. Numerical reconstruction

To simulate the visualisation of holograms by a user, the diffracted light wave is first propagated to the viewer plane with the angular spectrum. Then, it is cropped to fit the observer viewpoint and is finally back-propagated to the reconstruction plane. The brightness of each reconstruction varies widely, so each is normalized by the sum of its mean value and its standard deviation.

Figure 12 shows reconstructions computed from phase-only holograms generated with multi-view and view-specific approaches and quantized with a truncation method (Fig. 12a-b) and with the view-dependent error diffusion algorithm (Fig. 12c). The reconstruction of the multi-view hologram (Fig. 12(a)) has a poor quality as the conjugate order is superimposed on the right dices of the 3D scene. This artefact is far less perceptible in the reconstruction of the view-specific hologram. The perceptibility of the conjugate order decreases because only the light waves reaching the visualisation window are selected during the generation of view-specific holograms. In other words, this operation restricts the light waves propagation to a specific frequency range. Since the conjugate order of an hologram corresponds to a opposite frequency range with the same size, this artefact is reduced for view-specific hologram. This phenomenon is illustrated in Fig. 5. The view-dependent error diffusion algorithm also enhances the reconstruction quality by reducing the quantization error which improves the image contrast as illustrated in Fig. 12(c).

Figure 13 shows reconstructions focused at different depths which highlights that our method is able to accurately provide the accommodation depth cue. Furthermore, images in Fig. 14 show reconstructions of multi-view holograms and view-specific holograms with view-dependent error diffusion technique from several viewpoints. This experiment demonstrates that our approach selects a specific viewpoint. Indeed, two of the view-specific reconstructions only contain zero order and quantization noise that have been rejected outside the selected view.

To measure the brightness of each reconstruction, the mean intensity of the complex light field in the reconstruction plane is computed, as shown in Table 7. The reconstructions of the view-specific approach are brighter than the multi-view reconstruction since the light waves are concentrated in the viewing area. Furthermore, the reconstruction of the hologram quantized

Optics EXPRESS

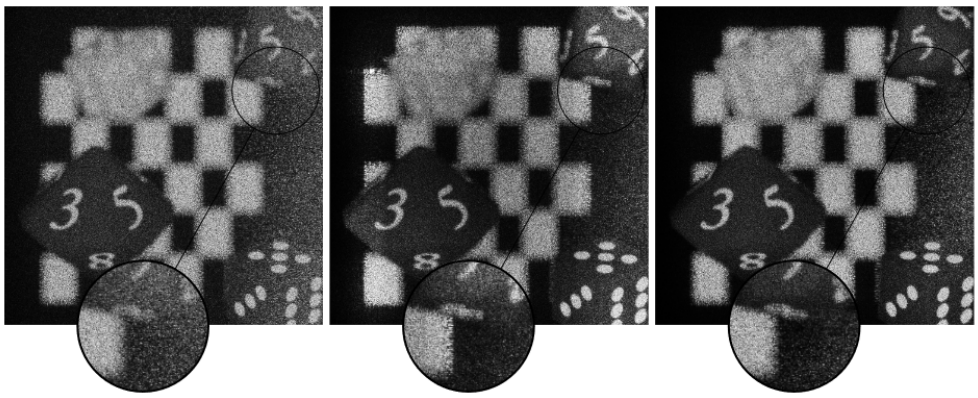

Fig. 12. (a) Reconstruction of a multi-view hologram quantized with a truncation method, (b) reconstruction of a view-specific hologram quantized with a truncation method and (c) reconstruction of a view-specific hologram quantized with the view-dependent error diffusion. Each hologram is a binary-phase signal.

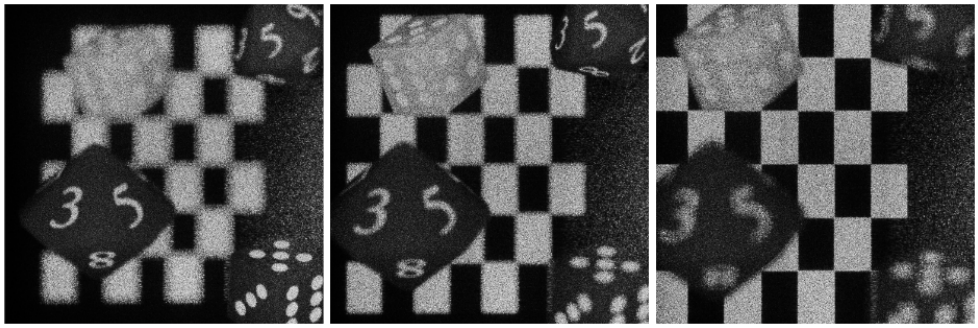

Fig. 13. Reconstructions of a view-specific hologram quantized on 2 levels with the view-dependent error diffusion focused at (a) 8.3cm, (b) 9.2cm, (c) 10.3cm.

with the view-dependent error diffusion algorithm is less bright because the quantization noise is rejected outside of the visualization window.

Table 7. Mean intensity of the reconstructions according to the hologram generation method.

Method	Mean intensity
Multi-view	0.014
View-specific	0.040
View-specific VDED	0.022

Table 8 shows objective quality evaluation of the holograms with peak signal-to-noise ratio (PSNR) and structural similarity (SSIM) metrics. The reference is a reconstruction of a multi-view hologram with floating-point complex values and the amplitude of each reconstruction is normalized. These results confirm that the view-specific VDED approach generates holograms of higher quality than the simple view-specific and the classic multi-view methods.

Optics EXPRESS

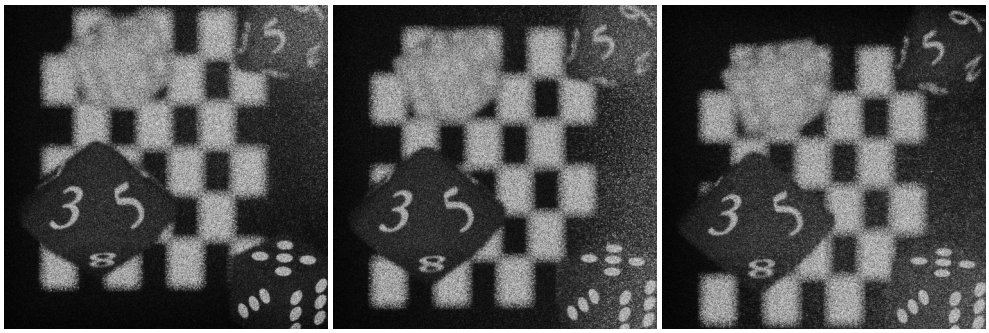

(a) Multi-view

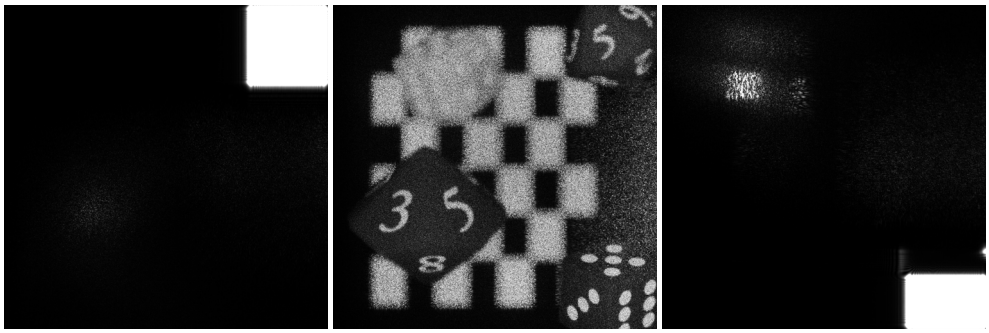

(b) View-specific VDED

Fig. 14. Reconstructions of binary a multi-view hologram and reconstructions of a view-specific hologram quantized on 2 levels with the view-dependent error diffusion algorithm from different point of views. Leftmost images are top views and rightmost images are bottom views.

Table 8. Objective evaluation of the reconstruction quality.

Phase levels (bits)	Multi-view		View-specific		View-specific VDED	
	PSNR	SSIM	PSNR	SSIM	PSNR	SSIM
1	12.89	0.35	13.53	0.40	15.57	0.51
8	19.93	0.59	15.78	0.50	20.91	0.75

5.5. Optical reconstruction

As our holograms contain more than 100 million of pixels, they cannot be displayed on conventional LCDs or DMDs. Hence, we engraved them in a clean room according to the following process. First, a layer of 1.6µm Microposit S1800 photoresist is spread on a 1.1µm glass plate by spin coating. Then, the resist is illuminated with the photoplotter presented in [37]. After exposure, it is developed by using the Microposit Developer 303A, which is diluted 1:12 in deionized water. Since this process allows up to 256 levels, the holograms were quantized on 8 bits.

To observe the 3D scene through the holograms, we use the test bench presented in Fig. 15. The holograms were illuminated by a polarized laser diode going trough a converging lens and a polarizer. The polarizer manages the illumination intensity and the converging lens allows the light waves that reach the hologram to be planar. The polarizer filters the light waves the same way for all the experiments. Reconstructions of the 3D scene were captured with a canon EOS 700D.

Optics EXPRESS

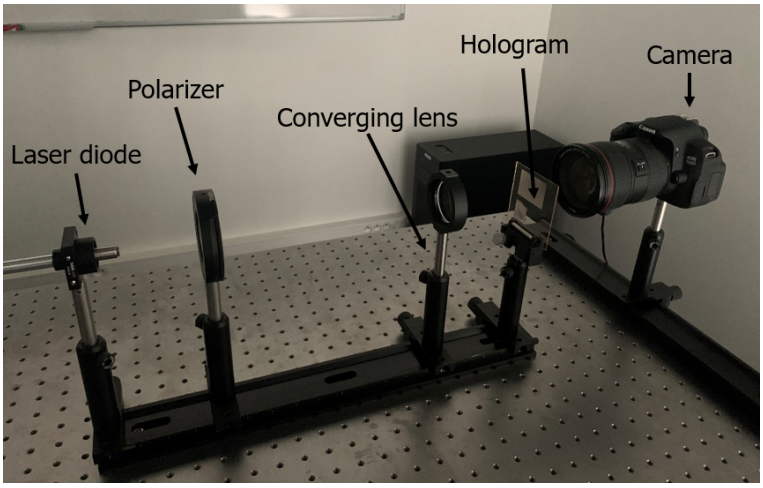

Fig. 15. Test bench to capture the 3D scene.

The parameters of the camera are the same for the photos of Fig. 16 and are described in Table 9. All the reconstructions contain a red dot which corresponds to the zero order. The multi-view reconstruction in Fig. 16(a) is less bright than the view-specific ones. In Fig. 16(b), the light intensity is concentrated on the edges of the reconstruction. This artefact is corrected in Fig. 16(c) by applying the VDED algorithm on the hologram. The exposure in the magnifications (black circle) is modified numerically in order to obtain a similar intensity for all the reconstructions. The magnification of the multi-view reconstruction contains more conjugate order than the view-specific ones which demonstrates its reduction by the use of our approach. Moreover, Visualization 1 illustrates a smooth continuity between views and a good depth information by showing the multi-view reconstruction at several depths and from several viewpoints. In this video, the camera is placed off-axis to remove the zero and conjugate orders.

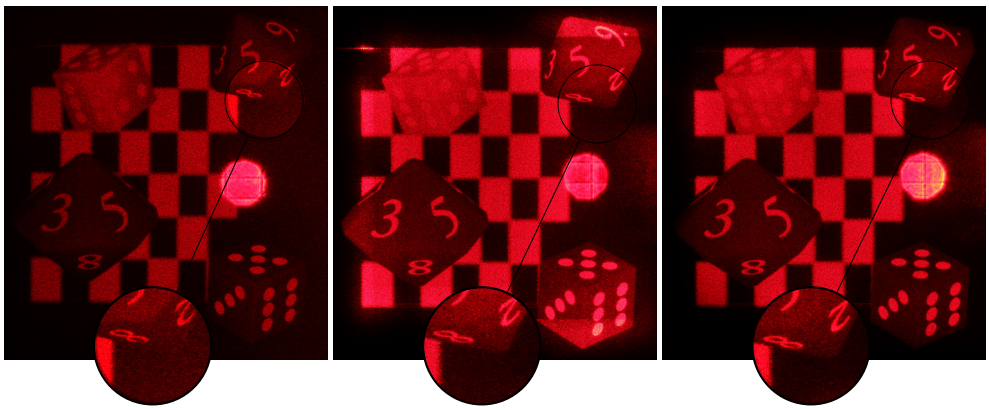

(a) Multi-view (b) View-specific (c) View-specific VDED

Fig. 16. (a) Optical reconstruction of a multi-view hologram quantized with a truncation method, (b) optical reconstruction of a view-specific hologram quantized with a truncation method and (c) optical reconstruction of a view-specific hologram quantized with the view-dependent error diffusion.

Optics EXPRESS

Table 9. Parameters of the camera. Photos are shown in Fig. 16 and the video in Visualization 1.

Parameter	Photo	Video
Exposure	1ms	1ms
Aperture size	8.75mm	25mm
ISO	100	100
Focal	70mm	70mm

6. Conclusion

In this paper, a novel view-specific layered-based stereogram approach including a view-dependent error diffusion algorithm is proposed. This method selects the light waves that are scattered to a specific viewing area during the generation process of the hologram and uses the view-dependent error diffusion technique to reject the quantization noise outside of the visualization window.

Experimental results demonstrate that our method is up to 94% faster than the layered holographic stereogram approach [27]. The quality of the view-specific reconstruction is also greatly improved as the conjugate order is significantly reduced, the 3D scene is 1.5 times brighter and the image contrast is improved.

Currently, the view-dependent error diffusion algorithm is slow because it is implemented on CPU and not optimized. However, in future work, we expect huge improvements in computation times as conventional state-of-the-art error diffusion techniques have already been implemented on GPU [45].

Funding. Agence Nationale de la Recherche (ANR-A0-AIRT-07).

Acknowledgment. The authors would like to thank Thomas Le Deun, IMT-Atlantique, for his support on the optical experiments.

Disclosures. The authors declare no conflicts of interest.

Data availability. Data underlying the results presented in this paper are not publicly available at this time but may be obtained from the authors upon reasonable request.

References

1. J. Carmigniani, B. Furht, M. Anisetti, *et al.*, "Augmented reality technologies, systems and applications," Multimed Tools Appl. **51**(1), 341–377 (2011).
2. C. Wheatstone, "Contributions to the physiology of vision.–part the first. on some remarkable, and hitherto unobserved, phenomena of binocular vision," Philos. Trans. R. Soc. London **128**, 371–394 (1838).
3. D. M. Hoffman, A. R. Girshick, K. Akeley, *et al.*, "Vergence-accommodation conflicts hinder visual performance and cause visual fatigue," Journal of Vision **8**(3), 33 (2008).
4. U. Schnars and W. Jüptner, *Digital Holography: Digital Hologram Recording, Numerical Reconstruction, and Related Techniques* (Springer Science & Business Media, 2005).
5. M. E. Lucente, "Interactive computation of holograms using a look-up table," J. Electron. Imaging **2**(1), 28–34 (1993).
6. S.-C. Kim and E.-S. Kim, "Effective generation of digital holograms of three-dimensional objects using a novel look-up table method," Appl. Opt. **47**(19), D55–D62 (2008).
7. Y. Pan, X. Xu, S. Solanki, *et al.*, "Fast CGH computation using S-LUT on GPU," Opt. Express **17**(21), 18543–18555 (2009).
8. T. Shimobaba, N. Masuda, and T. Ito, "Simple and fast calculation algorithm for computer-generated hologram with wavefront recording plane," Opt. Lett. **34**(20), 3133–3135 (2009).
9. K. Matsushima, H. Schimmel, and F. Wyrowski, "Fast calculation method for optical diffraction on tilted planes by use of the angular spectrum of plane waves," J. Opt. Soc. Am. A **20**(9), 1755–1762 (2003).
10. L. Ahrenberg, P. Benzie, M. Magnor, *et al.*, "Computer generated holograms from three dimensional meshes using an analytic light transport model," Appl. Opt. **47**(10), 1567–1574 (2008).
11. H. Kim, J. Hahn, and B. Lee, "Mathematical modeling of triangle-mesh-modeled three-dimensional surface objects for digital holography," Appl. Opt. **47**(19), D117–D127 (2008).
12. Y. Zhang, H. Fan, F. Wang, *et al.*, "Polygon-based computer-generated holography: a review of fundamentals and recent progress [Invited]," Appl. Opt. **61**(5), B363–B374 (2022).

Optics EXPRESS

13. M. Bayraktar and M. Özcan, "Method to calculate the far field of three-dimensional objects for computer-generated holography," Appl. Opt. **49**(24), 4647–4654 (2010).
14. Y. Zhao, L. Cao, H. Zhang, *et al.*, "Accurate calculation of computer-generated holograms using angular-spectrum layer-oriented method," Opt. Express **23**(20), 25440–25449 (2015).
15. J.-S. Chen and D. P. Chu, "Improved layer-based method for rapid hologram generation and real-time interactive holographic display applications," Opt. Express **23**(14), 18143–18155 (2015).
16. J. Jia, J. Si, and D. Chu, "Fast two-step layer-based method for computer generated hologram using sub-sparse 2D fast Fourier transform," Opt. Express **26**(13), 17487–17497 (2018).
17. T. Yamaguchi and H. Yoshikawa, "Computer-generated image hologram," Chin. Opt. Lett. **9**(12), 120006 (2011).
18. K. Matsushima and A. Kondoh, "Wave optical algorithm for creating digitally synthetic holograms of three-dimensional surface objects," Proc. SPIE **5005**, 190–197 (2003).
19. J.-P. Liu and H.-K. Liao, "Fast occlusion processing for a polygon-based computer-generated hologram using the slice-by-slice silhouette method," Appl. Opt. **57**(1), A215–A221 (2018).
20. J.-S. Chen, D. Chu, and Q. Smithwick, "Rapid hologram generation utilizing layer-based approach and graphic rendering for realistic three-dimensional image reconstruction by angular tiling," J. Electron. Imaging **23**(2), 023016 (2014).
21. T. Yatagai, "Stereoscopic approach to 3-D display using computer-generated holograms," Appl. Opt. **15**(11), 2722–2729 (1976).
22. H. Kang, T. Yamaguchi, and H. Yoshikawa, "Accurate phase-added stereogram to improve the coherent stereogram," Appl. Opt. **47**(19), D44–D54 (2008).
23. M. Yamaguchi, H. Hoshino, T. Honda, *et al.*, "Phase-added stereogram: calculation of hologram using computer graphics technique," Proc. SPIE **1914**, 25–31 (1993).
24. S. Igarashi, T. Nakamura, and M. Yamaguchi, "Fast method of calculating a photorealistic hologram based on orthographic ray-wavefront conversion," Opt. Lett. **41**(7), 1396–1399 (2016).
25. K. Wakunami and M. Yamaguchi, "Calculation for computer generated hologram using ray-sampling plane," Opt. Express **19**(10), 9086–9101 (2011).
26. Q. Y. J. Smithwick, J. Barabas, D. E. Smalley, *et al.*, "Interactive holographic stereograms with accommodation cues," Proc. SPIE **7619**, 761903 (2010).
27. H. Zhang, Y. Zhao, L. Cao, *et al.*, "Layered holographic stereogram based on inverse Fresnel diffraction," Appl. Opt. **55**(3), A154–A159 (2016).
28. F. Yaras, H. Kang, and L. Onural, "State of the Art in Holographic Displays: A Survey," J. Disp. Technol. **6**(10), 443–454 (2010).
29. V. Kettunen, "Review of iterative Fourier-transform algorithms for beam shaping applications," Opt. Eng. **43**(11), 2549–2556 (2004).
30. H. Song, G. Sung, S. Choi, *et al.*, "Optimal synthesis of double-phase computer generated holograms using a phase-only spatial light modulator with grating filter," Opt. Express **20**(28), 29844–29853 (2012).
31. C.-H. Ting, K. Wakunami, K. Yamamoto, *et al.*, "Reconstruct holographic 3D objects by double phase hologram," Proc. SPIE **9495**, 94950V (2015).
32. M. El Bouz and K. Heggarty, "Signal window minimum average error algorithm for multi-phase level computer-generated holograms," Opt. Commun. **180**(1-3), 21–28 (2000).
33. K. Liu, Z. He, and L. Cao, "Pattern-adaptive error diffusion algorithm for improved phase-only hologram generation," Chin. Opt. Lett. **19**(5), 050501 (2021).
34. H. Pang, J. Wang, M. Zhang, *et al.*, "Non-iterative phase-only Fourier hologram generation with high image quality," Opt. Express **25**(13), 14323–14333 (2017).
35. R. Häussler, Y. Gritsai, E. Zschau, *et al.*, "Large real-time holographic 3D displays: enabling components and results," Appl. Opt. **56**(13), F45–F52 (2017).
36. T. Kozacki, "On resolution and viewing of holographic image generated by 3D holographic display," Opt. Express **18**(26), 27118–27129 (2010).
37. M. V. Kessels, "Versatile stepper based maskless microlithography using a liquid crystal display for direct write of binary and multilevel microstructures," J. Micro/Nanolithogr., MEMS, MOEMS **6**(3), 033002 (2007).
38. S. Weissbach, F. Wyrowski, and O. Bryngdahl, "Digital phase holograms: Coding and quantization with an error diffusion concept," Opt. Commun. **72**(1-2), 37–41 (1989).
39. R. Eschbach, "Comparison of error diffusion methods for computer-generated holograms," Appl. Opt. **30**(26), 3702–3710 (1991).
40. K. Heggarty and R. Chevallier, "Signal window minimum average error algorithm for computer-generated holograms," J. Opt. Soc. Am. A **15**(3), 625–635 (1998).
41. P. W. M. Tsang and T.-C. Poon, "Novel method for converting digital Fresnel hologram to phase-only hologram based on bidirectional error diffusion," Opt. Express **21**(20), 23680–23686 (2013).
42. K. Matsushima and S. Nakahara, "Extremely high-definition full-parallax computer-generated hologram created by the polygon-based method," Appl. Opt. **48**(34), H54–H63 (2009).
43. J. W. Goodman, *Introduction to Fourier optics / Joseph W. Goodman.* (Roberts & Co., Englewood, Colo, 2005), chap. 4.2.2 Accuracy of the Fresnel approximation, pp. 68–72, 3rd ed.

Optics EXPRESS

44. A. Gilles and P. Gioia, "Real-time layer-based computer-generated hologram calculation for the Fourier transform optical system," Appl. Opt. **57**(29), 8508–8517 (2018).
45. S. Funasaka, K. Nakano, and Y. Ito, "Single Kernel Soft Synchronization Technique for Task Arrays on CUDA-enabled GPUs, with Applications," in *2017 Fifth International Symposium on Computing and Networking (CANDAR)*, (IEEE, Aomori, 2017), pp. 11–20.